BOLETIN DE LA SOCIEDAD ESPAÑOLA DE
Cerámica y Vidrio
www.elsevier.es/bsecv

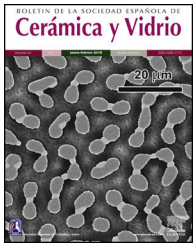

Synthesis of nano-crystalline forsterite (Mg_2SiO_4) powder from biomass rice husk silica by solid-state route

*Lakshya Mathur**, *S.K. Saddam Hossain*, *Manas R. Majhi*, *Pradip K. Roy*

Department of Ceramic Engineering, IIT-BHU, Varanasi 221005, India

ARTICLE INFO

Article history:
Received 6 March 2017
Accepted 3 October 2017
Available online 31 October 2017

Keywords:
Solid state synthesis
Amorphous silica
Rice husk (RH)
Rice husk ash (RHA)
Forsterite
Waste material

ABSTRACT

The aim of the investigation is to develop nano-crystalline forsterite by utilizing amorphous silica and magnesia through solid-state route. Amorphous silica was yielded from burning of biomass, i.e. rice husk (RH). The precursor and powders were subjected to calcination for a temperature range of 700–1000 °C and evolution of forsterite phase was characterized using Fourier transform infrared (FTIR) spectroscopy, X-ray diffraction (XRD), and scanning electron microscopy (SEM). The results indicate that by increasing temperature around 1000 °C, magnesia and amorphous silica were absolutely consumed and turned into a single forsterite phase. Crystal size was calculated by XRD analysis (80–85 nm) and particle size was determined by SEM micrograph analysis, which reveals that prepared powder consist particles with nearly spherical morphology, and mean particle size of 265 nm.

Síntesis de polvo de forsterita nanocristalina (Mg_2SiO_4) a partir de sílice de cáscara de arroz de biomasa por vía de estado sólido

Palabras clave:
Síntesis de estado sólido
Sílice amorfa
Cáscara de arroz
Ceniza de cáscara de arroz
Forsterita
Material de desecho

RESUMEN

El objetivo de la investigación es desarrollar forsterita nanocristalina mediante la utilización de sílice amorfa y magnesia a través de la vía de estado sólido. La sílice amorfa se obtuvo por combustión de biomasa, es decir, a partir de cáscara de arroz. El precursor y los polvos se sometieron a calcinación en un intervalo de temperaturas de 700–1.000 °C y la evolución de la fase forsterita se calificó mediante espectroscopia infrarroja por transformadas de Fourier (FTIR), difracción de rayos X (XRD) y microscopia electrónica de barrido (SEM). Los resultados indican que, al aumentar la temperatura a unos 1.000 °C, la magnesia y la sílice

* *Corresponding author.*
E-mail address: mrmmajhi.cer@itbhu.ac.in (L. Mathur).
https://doi.org/10.1016/j.bsecv.2017.10.004

amorfa se consumieron totalmente y se convirtieron en una fase de forsterita única. El tamaño del cristal se calculó mediante análisis de XRD (80-85 nm) y el tamaño de la partícula se determinó mediante análisis de micrografía SEM, lo que revela que el polvo preparado contiene partículas con una morfología casi esférica y un tamaño medio de partícula de 265 nm.

Introduction

Nano materials are eminent as the vital materials in nanotechnology due to their exclusive properties including high strength, high hardness, extremely high diffusion rates, and therefore reduced sintering times in comparison to the conventional coarse grain materials [1–4].

Crystalline magnesium silicate with chemical formula Mg_2SiO_4 is a mineral phase recognized as forsterite, named after the German scientist Johann Forster. Forsterite is predominately consists of the anion SiO_4^{4-} and the cation Mg^{2+} in a molar ratio 1:2 and relates to the group of olivines [5]. It also exhibits good refractoriness due to its high melting point (1890 °C), low dielectric permittivity, low thermal expansion, extremely low electrical conductivity, good chemical stability and excellent insulation properties even at high temperatures. It is insulating in nature with very low thermal conductivity compared to pure MgO (about 1/3–1/4 of the pure MgO) [6–9]. All of these characteristics stated above make it relevant material for engineers and designers to use them in the fabrication of numerous technical components such as refractory materials [10–12], dielectric substrates [13,14], solid oxide fuel cells (SOFC) [15,16], optical devices [17], pigments [18], biomaterials [19,20], composite materials [10,21,22], electronics and tunable laser [23].

Previous researchers utilized diverse methods to evolve high purity forsterite phase such as co-precipitation [24], polymer precursor [25], sol–gel [26–28] and mechanical activation [29–31]. This evolution of high purity forsterite phase is strongly depends on firing temperature [32,33]. It was reported that firing temperature has been changed as the process for fabrication of same has change, such as 800 °C for co-precipitation, polymer precursor, citrate-nitrate routs (sol–gel), above 1000 °C for heterogeneous sol–gel route and 1000–1200 °C for mechanical activation. However, these methods cannot be used for comprehensive industrial production of high purity forsterite due to their high cost.

In last few decades forsterite was prepared with various ingredients such as serpentine [11], olivine [34], iron ore tailing [35], zeolite and MgO [15] talc and magnesium carbonate [36] or MgO [37], and MgO with silica [38]. Another raw material for evolution of ceramic is 'rice husk' (RH) because it incorporates a huge amount of silica and is redundantly available. RH is a renewable source of silica and extraction of silica from it, is also easy. Burnt product of rice husk is rice husk ash (RHA). Silica found from RH was used for preparation of borosilicate, cordierite, carbosil, alumino-silicate and mullite [39–44]. The potential of rice husk as an excellent source of high-grade amorphous silica has also been investigated in many other studies [45–47]. This amorphous silica can be utilized for preparation of solar grade silicon, silicon carbide, magnesium–alumina–silica, and lithium–aluminum–silica [48–51].

Abundant availability and high content of silica make RH relevant ingredient to be utilized in forsterite preparation. Another ingredient for preparation of forsterite, i.e. magnesia was added in form of dead burnt magnesia (DBM). The present study is aimed to the appraisal of, formation of nanocrystalline forsterite by using rice husk as a source of silica by solid state route.

Materials and experimental

Biomass in form of rice husk (RH) was acquired from rice mill. RH was dried at 50 °C and then sear in an open environment, this burning of biomass yield rice husk ash (RHA). RHA was further grounded and heat treated at 600 °C for 4 h, due to the presence of trace amount of unburnt carbon. Chemical, mineralogical and morphological characteristics of rice husk were dynamically influenced by rice diversity, soil chemistry, climatic conditions, and geographic localization of the culture [52,53]. The chemical composition of RHA was analyzed by the X-ray fluorescence spectrometer (XRF) according to ASTM C114-00 [54] shown in Table 1. It was found that RHA incorporates 96% of SiO_2. The XRD analysis was carried out for RHA and the results were recorded in the range of 10–90° for 2, θ shown in Fig. 1. The absence of any sharp peak illustrates that the silica in the RHA is in amorphous form only. The amorphous silica present in RHA is also known as active silica, which is consider to be more reactive than the crystalline one, because it has short-range order characteristic of a crystal [46]. Amorphous materials have an internal structure made of interconnected structural blocks. Analytical grade (assay 99%) dead burnt magnesia (DBM) was purchased from Lobachemie Pvt. Ltd., India, which contains periclase as its major phase.

Table 1 – Chemical composition by XRF of heat treated RHA.

Compound	Wt.%	Compound	Wt.%
SiO_2	96.01	TiO_2	0.08
Na_2O	1.42	ZnO	0.07
P_2O_5	0.91	CuO	0.06
K_2O	0.52	Rb_2O	0.03
CaO	0.42	BaO	0.02
Fe_2O_3	0.16	ZrO_2	0.02
MgO	0.11	Re_2O_7	0.01
RuO_2	0.10	Y_2O_3	0.01
SO_3	0.09	Eu_2O_3	0.01

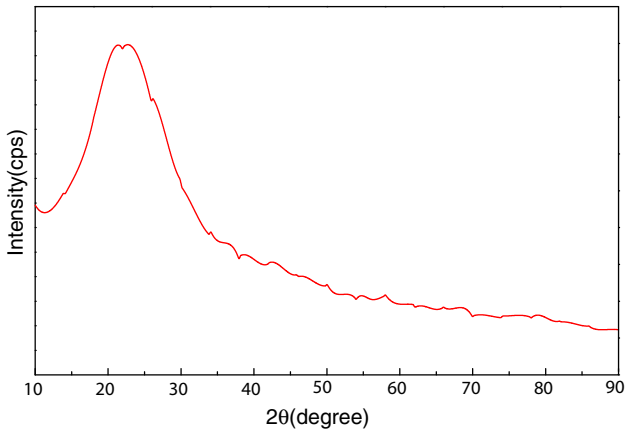

Fig. 1 – XRD of heat treated RHA.

In the present work initially all raw materials were crushed and grind up to fine particle size (45 μm). Screened materials were taken into a stoichiometric amount shown in Table 2 and then pulverized in a high speed ball mill for 300 rpm in absolute alcohol medium using Zirconia balls of 10 mm diameter for 12 h. Balls to powder weight ratio was kept 5:1. The mixture was then dried, grind and calcined on 700 °C (T-1), 800 °C (T-2), 900 °C (T-3), 1000 °C (T-4), with a ramp rate of 5 °C/min for 2 h in air atmosphere [55].

In order to investigate crystal size, surface morphology, particle size and phase formation, various tests were executed using different equipment. In order to identify the crystalline forsterite phase present in the calcined powder, it was subjected to X-ray diffraction analysis (XRD) using RIGAKU-Miniflex II diffractometer (Serial no: HD20972, Japan) adopted Cu Kα radiation (λ = 1.5405 Å) with a tube voltage of 40 kV and current of 35 mA in a 2θ range between 10° and 90°. During measurement the step size and speed were set to 0.02° and 1° per min, respectively and were followed in the present investigation. The JCPDS-International Centre for diffraction Data Cards were used as a reference. The crystallite sizes of the calcined powder samples were determined from X-ray line broadening using the Sherrer's equation as follows:

$$t = \frac{0.9\lambda}{(B\cos\theta)} \quad (1)$$

where t is the crystallite size, λ is the wavelength of the radiation, θ is the Bragg's angle and B is the full width at half maximum. To determine the mean crystallite size of synthesized forsterite three diffraction peaks were considered, i.e. (011), (112) and (400). Line broadening due to the instrument was subtracted from the peak width before calculating the crystallite size using the following formula:

$$B^2 = B_{meas}^2 - B_{equip}^2 \quad (2)$$

where B_{meas} = measured full width at half maximum from peak, B_{equip} = instrumental broadening. The molecular structure of the fired powder was studied using Fourier transform infrared spectroscopy (BRUKER, TENSOR 27-3772) between 4000 and 400 cm^{-1} through attenuated total reflection (ATR) method. The surface morphology of the forsterite refractory was examined using SEM (ZEISS, EVO 18-2045). Particle size estimated from SEM micrograph by software entitled as "Image J1.48V".

Table 2 – Proportion and average particle size of the raw materials.

Raw materials	MgO	Amorphous silica
Proportion (wt.%)	57	43
Particle size (μm)	45	45

Result and discussion

To reveal the phase transformation occurs during heat treatment powders were characterized by X-ray diffraction method. XRD patterns of the various samples calcined at different temperature demonstrated in Fig. 2(A)–(D). Indexing of phases was completed with the help of JCPDS file no. 34-0189, it displays the existence of forsterite phase with the most intense peak at 2θ = 20.6°, 41.80°, and 62.008° having reflections from (011), (112), (400) planes respectively; similar results were found in previous studies [14,15,55]. Some peaks of other phases were also found at low temperature that was eliminated by the escalation of temperature up to 1000 °C. These low temperature phases were periclase, enstatite and clinoenstatite, identified by JCPDS file no: 43-1022, 19-0768, 35-0610 respectively. Fig. 2(A) shows that

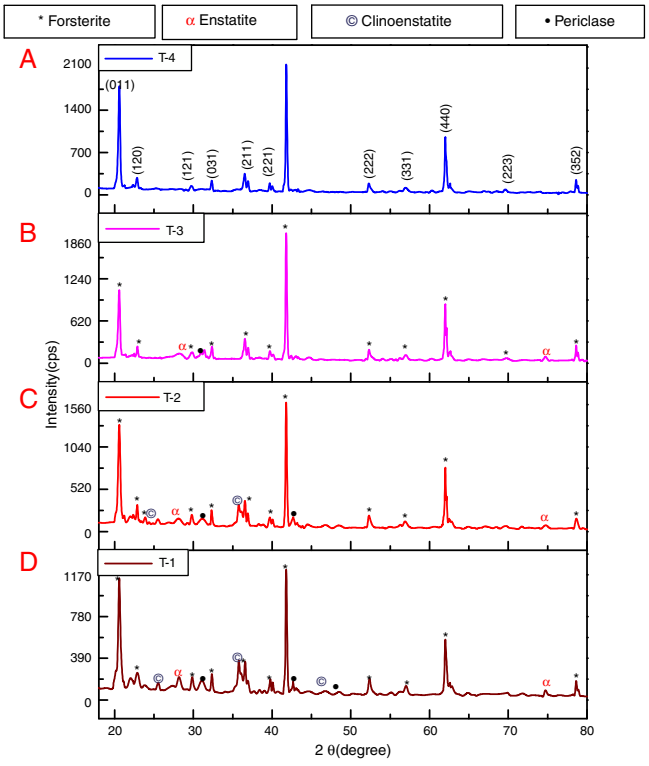

Fig. 2 – XRD of (A) T-4, (B) T-3, (C) T-2, (D) T-1.

Table 3 – Mean crystallite and particle size of samples.

Sample	Temperature (°C)	Crystal size at different peak (hkl) ± 2 (nm)			Mean crystallite size ± 2 (nm)	Standard deviation for crystallite size (σ)	Mean particle size ± 2(nm)
		(011)	(112)	(400)			
T-1	700	53	103	84	80	11.90	221
T-2	800	51	98	93	81	12.17	255
T-3	900	58	100	94	84	10.71	289
T-4	1000	57	105	94	85	11.85	298

maximum intensity peak occurs only when powder was calcined at 1000 °C, this maximum intensity peak correspond to pure forsterite phase formation. First of all magnesium oxide was constituted in the structure then the reaction between this magnesium oxide and SiO_2 at the surface causes formation of enstatite and clinoenstatite. Further, due to diffusion of magnesia in enstatite or clinoenstatite, forsterite phase was constituted. Consequences of shortfall in particle size are, increase in homogeneous powder that results faster formation of forsterite structure at lower temperature. Due to this diffusion mechanism other phases such as periclase and amorphous silica were completely absent in the powder that was calcined at 1000 °C.

In addition to analysis of crystal system, the lattice parameter and mean crystallite size of the powder was calculated. Lattice parameter was found by indexing of dominating peaks made in XRD analysis. Lattice parameter found are identical to the orthorhombic Mg_2SiO_4 structure, which is consistent with the standard data file (JCPDS file card no: 34-0189). Lattice parameter is a(Å) = 5.98, b(Å) = 10.01, c(Å) = 4.78 and unit cell volume (Å^3) = 286.69 supported by previous studies [56]. Mean crystallite size was calculated from the peak broadening in a XRD diffraction pattern associated with a particular planar reflection from within the crystal unit cell based on Scherrer's formula Eq. (1). In the present investigation, the crystallite size was calculated from 2θ corresponding to the three dominating peaks of forsterite at approximately 20.6°, 41.80°, and 62.008°. Mean crystallite size of resulted powders at different calcination temperatures are included in Table 3. As shown in table mean crystal size was raised as the calcination temperature augmented. Initially variation in crystal size from 700 °C to 800 °C was very low, but as the temperature raises the mean crystal size fluctuates from 80 nm to 85 nm calculated from Fig. 2. This fluctuation in crystal size indicates the formation of single crystal forsterite. Here crystal size was found in a nano-size range that illuminates the formation of nano-crystalline forsterite particles, supported by lattice parameter.

In order to study the creation of chemical bonds during milling and calcination, powders were subjected to FTIR test. Fig. 3 illustrates FT-IR spectra of powders fired at discrete temperatures, i.e. 700 °C, 800 °C, 900 °C and 1000 °C. All the IR bands traced are displayed in Table 4 with their corresponding functional group. FTIR analysis was used to follow the formation of crystalline forsterite, SiO_4, Si—O—Si bond, MgO_6 Modes and MgO bands. In fired samples the intense bands concerned with the characteristic peaks of forsterite appear in the range of 830–880 cm^{-1}, 1010–1030 cm^{-1}. Identical results were also reported in previous studies [15]. Few characteristics bands of forsterite also traced in the range

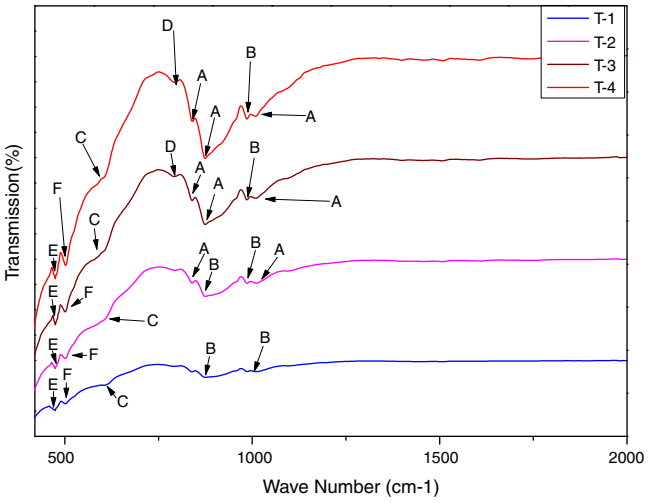

Fig. 3 – Infrared transmission spectra of calcined samples.

Table 4 – Symbol used for FTIR peaks and corresponding functional group.

Symbol	Peak (cm^{-1})	Functional group
A	830–880, 1010–1030	Crystalline forsterite
B	980–1000, 860–890	SiO_4 (stretching)
C	600–615	SiO_4 (bending)
D	780–820	Si—O—Si (stretching)
E	475–477	MgO_6 modes
F	500–505	MgO (stretching)

of 980–1000 cm^{-1}, 860–890 cm^{-1} and 600–615 cm^{-1} associated to SiO_4 stretching and SiO_4 bending modes respectively [27]. Bands around 475–477 cm^{-1} are concerned to octahedral MgO_6 modes [25,27,57]. These peaks justify the formation of forsterite as it is shown in XRD pattern of the samples. A few bands were associated with MgO stretching mode in the range of 500–505 [15]. Downfall found in the range of 780–820 cm^{-1} corresponding to Si—O—Si symmetric stretching vibrations [57].

The surface morphologies of the powder calcined at discrete temperature, i.e. 700 °C, 800 °C, 900 °C and 1000 °C were studied using scanning electron microscope (SEM). The micrographs displayed in Fig. 4(a)–(d). Micrographs demonstrate a significant effect of temperature variation on the size and distribution of the particles on the surface. Fig. 4(a) indicate that after calcination at 700 °C, no particle coarsening occurred and the shape and size stand almost same as those of milled powder shown in Fig. 5. But as the temperature augmented up to 1000 °C, the particle size lightly increased as a function of

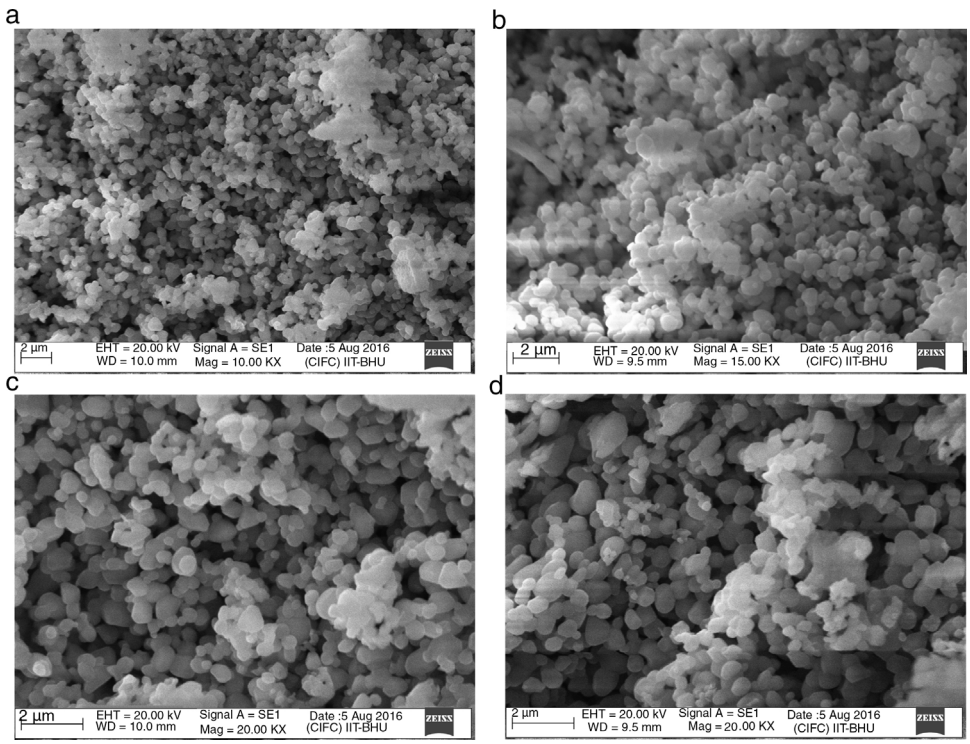

Fig. 4 – Scanning electron microscopy (SEM) images of the sample calcined at different temperatures (a) 700 °C, (b) 800 °C, (c) 900 °C, (d) 1000 °C.

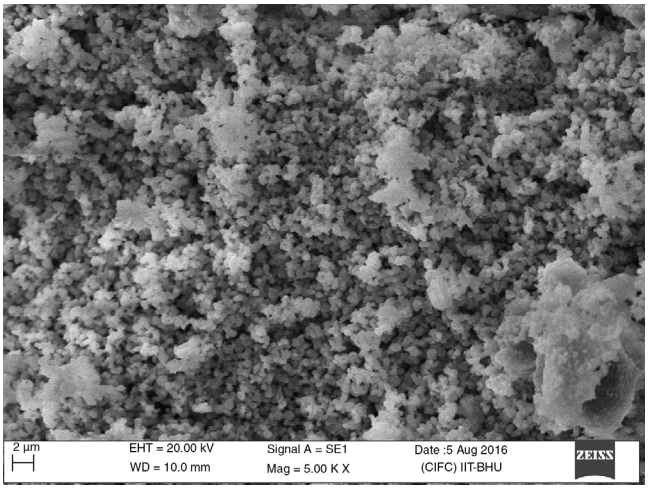

Fig. 5 – SEM micrograph of milled sample.

calcination temperature indicated in Fig. 4(d). Mean particle size of calcined powder was determined using "linear intersection method" on SEM micrographs was found in the range of 221–298 nm shown in Table 3.

Energy dispersive spectroscopy or EDX analysis of T-4 is demonstrated in Fig. 6. The theoretical value of Mg, Si, and Oxygen in forsterite is 34.54%, 19.96%, 45.49% respectively. Fig. 6 shows that the amount of Mg, Si, and oxygen in T-4 is approximately identical to theoretical values of the same in forsterite. This shows there is an absence of free periclase or free silica in sample, i.e. periclase and silica were completely reacted and transformed into forsterite phase.

Conclusions

Nanocrystalline forsterite (Mg_2SiO_4) was synthesized by solid state route using rice husk as biomass and magnesium oxide as ingredient. Samples were calcined at various temperatures ranging from 700 °C to 1000 °C. Erection of forsterite phase begin from 700 °C and single- phase crystallite forsterite was acquired at 1000 °C. Combination of biomass and solid state route yield nano-crystallite forsterite phase having crystallite and particle size in the range of 50–105 nm and less than 300 nm respectively. This combination leads to much easier and cheaper way for fabrication of nano-crystallite forsterite particles than other one, so this one can be used for bulk production of the same.

Acknowledgement

We are beholden to the Faculties, Staff, Head of the Department of Ceramic Engineering, and Director of IIT-BHU, Varanasi, India for providing the adequate facilities to effectuate this work.

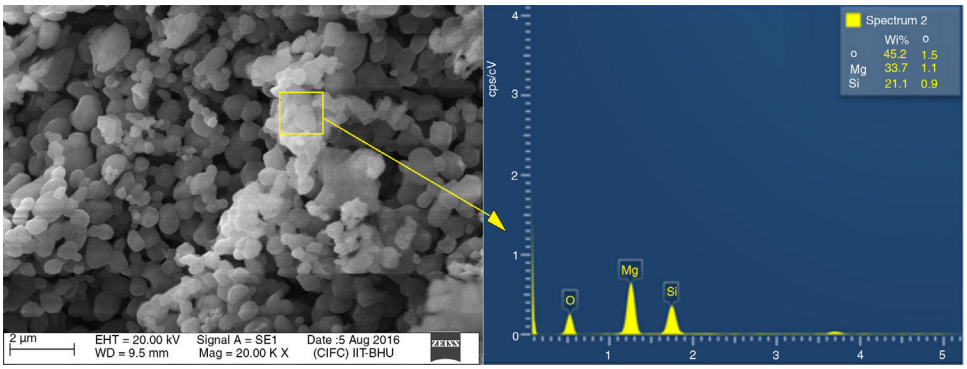

Fig. 6 – EDX spectra of the sample designed as T-4.

REFERENCES

[1] C. Suryanarayana, Mechanical alloying and milling, Prog. Mater. Sci. 46 (2001) 1–184.
[2] M. Tavoosi, M.H. Enayati, F. Karimzadeh, Softening behaviour of nanostructured Al–14 wt% Zn alloy during mechanical alloying, J. Alloys Compd. 464 (2008) 107–110.
[3] Z. Lei, Z. Liu, Y. Chen, Cyclic hydrogen storage properties of Mg milled with nickel nano-powders and Ni, J. Alloys Compd. 470 (2009) 470–472.
[4] G.L. Tan, J.H. Du, Q.J. Zhang, Structural evolution and optical properties of CdSe nanocrystals prepared by mechanical alloying, J. Alloys Compd. 468 (2009) 421–431.
[5] I. Kazuaki, Lattice dynamics of forsterite, Am. Miner. 63 (1978) 1198–1208.
[6] G.W. Brindley, R. Hayami, Kinetics and mechanism of formation of forsterite (Mg_2SiO_4) by solid state reaction of MgO and SiO_2, Philos. Mag. Lett. 12 (1965) 505.
[7] J.H. Chesters, Refractories Production and Properties, The Iron and Steel Institute, London, 1973.
[8] M.I. Diesperova, V.A. Bron, V.A. Perepelitsyn, T.I. Boriskova, V.A. Alekseeva, E.I. Kelareva, Forsterite refractories from the dunites of the Kytlym deposits, Refract. Ind. Ceram. 18 (1977) 278.
[9] P.K. Xu, G.Z. Wei, New Process Technology for Refractory, Metallurgy Industry Press, Beijing, 2005, pp. 46–47.
[10] E. Mustafa, N. Khalil, A. Gamal, Sintering and microstructure of spinel forsterite bodies, Ceram. Int. 28 (2002) 663–667.
[11] T.W. Cheng, Y.C. Ding, J.P. Chiu, A study of synthetic forsterite refractory materials using waste serpentine cutting, Miner. Eng. 15 (2002) 271–275.
[12] S.K.S. Hossain, L. Mathur, P. Singh, M.R. Majhi, Preparation of forsterite refractory using highly abundant amorphous rice husk silica for thermal insulation, J. Asian Ceram. Soc. 5 (2017) 82–87.
[13] K.X. Song, X.M. Chen, X.C. Fan, Effects of Mg/Si ratio on microwave dielectric characteristics of forsterite ceramics, J. Am. Ceram. Soc. 90 (2007) 1808–1811.
[14] T.S. Sasikala, M.N. Suma, P. Mohanan, C. Pavithran, M.T. Sebastian, Forsterite based ceramic glass composites for substrate applications in microwave and millimeter wave communications, J. Alloys Compd. 461 (2008) 555–559.
[15] F.C. Kosanovic, N. Stubicar, N. Tomasic, V. Bermanec, M. Stubicar, Synthesis of a forsterite powder by combined ball milling and thermal treatment, J. Alloys Compd. 389 (2005) 306–309.
[16] K.P. Sanosh, A. Balakrishnan, L. Francis, T.N. Kim, Sol–gel synthesis of forsterite nanopowders with narrow particle size distribution, J. Alloys Compd. 495 (2010) 113–115.
[17] T. Tani, S. Saeki, T. Suzuki, Y. Ohishi, Chromium-doped forsterite nanoparticle synthesis by flame spray pyrolysis, J. Am. Ceram. Soc. 90 (2007) 805–808.
[18] M. El Hadri, H. Ahamdane, M.A. El Idrissi Raghni, Sol gel synthesis of forsterite, M-doped forsterite (M = Ni, Co) solid solutions and their use as ceramic pigments, J. Eur. Ceram. Soc. 35 (2015) 765–777.
[19] S. Ni, L. Chou, J. Chang, Preparation and characterization of forsterite (Mg_2SiO_4) bio ceramics, Ceram. Int. 33 (2007) 83–88.
[20] M.A. Naghiu, M. Gorea, E. Mutch, F. Kristaly, M. Tomoaia-Cotisel, Forsterite nanopowder: structural characterization and biocompatibility evaluation, J. Mater. Sci. Technol. 29 (2013) 628–632.
[21] F. Tavangarian, R. Emadi, Synthesis and characterization of spinel forsterite nanocomposites, Ceram. Int. 37 (2011) 2543–2548.
[22] A. Teimouri, L. Ghorbanian, A. Najafi Chermahini, R. Emadi, Fabrication and characterization of silk/forsterite composites for tissue engineering applications, Ceram. Int. 40 (2014) 6405–6411.
[23] V. Petricevic, S.K. Gayen, R.R. Alfano, K. Yamagishi, Laser action in chromium-doped forsterite, Appl. Phys. Lett. 52 (1988) 1040.
[24] O. Yamaguchi, Y. Nakajima, K. Shimizu, Formation of forsterits ($2MgO{\cdot}SiO_2$) from the mixture prepared by alkoxy-method, Chem. Lett. 5 (1976) 401–404.
[25] A. Saberi, B. Alinejad, Z. Negahdari, F. Kazemi, A. Almasi, A novel method to low temperature synthesis of nano crystalline forsterite, Mater. Res. Bull. 42 (2007) 666–673.
[26] A. Saberi, Z. Negahdari, B. Alinejad, F. Golestani-Fard, Synthesis and characterization of nano crystalline forsterite through citrate–nitrate route, Ceram. Int. 35 (2009) 1705–1708.
[27] M.T. Tsai, Synthesis of nanocrystalline forsterite fibre via a chemical route, Mater. Res. Bull. 37 (2002) 2213–2226.
[28] T. Shiono, R. Sato, H. Shiomi, T. Minagi, T. Nishida, Synthesis and characterization of forsterite precursor-effects of milling precursors on its crystallization and reactivity, J. Soc. Mater. Sci. Jpn. 48 (1999) 554–558.
[29] M.H. Fathi, M. Kharaziha, Mechanically activated crystallization of phase pure nano crystalline forsterite powders, Mater. Lett. 62 (2008) 4306–4309.
[30] F. Tavangarian, R. Emadi, A. Shafyei, Influence of mechanical activation and thermal treatment time on nano particle forsterite formation mechanism, Powder Technol. 198 (2010) 412–416.
[31] F. Tavangarian, R. Emadi, Effects of fluorine ion and mechanical activation on nano structure forsterite formation mechanism, Powder Technol. 203 (2010) 180–186.

[32] M. Ando, K. Himura, T. Tsunooka, I. Kagomiya, H. Ohsato, Synthesis of high-quality forsterite, Jpn. J. Appl. Phys. 46 (2007) 7112.
[33] S. Sano, N. Saito, S. Matsuda, N. Ohashi, H. Haneda, Y. Arita, M. Takemoto, Synthesis of high density and transparent forsterite ceramics using nanosized precursors and their dielectric properties, J. Am. Ceram. Soc. 89 (2006) 568–574.
[34] R. Sarkar, R.K. Sinha, Development of forsterite refractories from Indian olivine, Trans. Indian Ceram. Soc. 61 (1) (2002) 20–25.
[35] L.I. Jing, W.A.N.G. Qi, L.I.U. Jihui, L.I. Peng, Synthesis process of forsterite refractory by iron ore tailings, J. Environ. Sci. Suppl. (2009) S92–S95.
[36] F. Tavangarian, R. Emadi, Mechanical activation assisted synthesis of pure nanocrystalline forsterite powder, J. Alloys Compd. 485 (2009) 648–652.
[37] F. Tavangarian, R. Emadi, Synthesis of nanocrystalline forsterite (Mg_2SiO_4) powder by combined mechanical activation and thermal treatment, Mater. Res. Bull. 45 (2010) 388–391.
[38] L. Cheng, P. Liu, X. Chen, W. Niu, G. Yao, C. Liu, X. Zhao, Q. Liu, H. Zhang, Fabrication of nanopowders by high energy ball milling and low temperature sintering of Mg_2SiO_4 microwave dielectrics, J. Alloys Compd. 513 (2012) 373–377.
[39] S. Sembiring, Synthesis and characterization of rice husk silica based borosilicate (B_2SiO_5) ceramic by sol–gel routes, Indones. J. Chem. 11 (1) (2011) 85–89.
[40] W. Simanjuntak, S. Sembiring, The use of the rietveld method to study the phase composition of cordierite ($Mg_2Al_4Si_5O_{18}$) ceramics prepared from rice husk silica, Makara J. Sci. 15 (1) (2011) 97–100.
[41] W. Simanjuntak, S. Sembiring, K. Sebayang, Effect of pyrolysis temperature on composition and electrical conductivity of carbosil prepared from rice husk, Indones. J. Chem. 12 (1) (2012) 119–125.
[42] W. Simanjuntak, S. Sembiring, P. Manurung, R. Situmeang, I.M. Low, Characteristics of aluminosilicates prepared from rice husk silica and aluminum metal, Ceram. Int. 39 (8) (2013) 9369–9375.
[43] S. Sembiring, W. Simanjuntak, X-ray diffraction phase analyses of mullite derived from rice husk silica, Makara J. Sci. 16 (2) (2012) 77–82.
[44] S. Sembiring, W. Simanjuntak, P. Manurung, D. Asmi, I.M. Low, Synthesis and characterization of gel-derived mullite precursors from rice husk silica, Ceram. Int. 40 (5) (2014) 7067–7072.
[45] A.A.M. Daifullah, N.S. Awwad, S.A. El-Reefy, Purification of phosphoric acid from ferric ion using modified rice husk, J. Chem. Eng. Proc. 43 (2004) 193–201.
[46] V.P. Della, I. Kuhn, D. Hotza, Rice husk ash an alternate source for active silica production, Mater. Lett. 57 (2002) 818–821.
[47] K. Amutha, R. Ravibaskar, G. Sivakumar, Extraction, synthesis and characterisation of nano silica from rice husk ash, Int. Nanotechnol. Appl. 4 (1) (2010) 61–66.
[48] M. Subarna, P. Banerjee, S. Purakayasha, B. Ghosh, Silicon-doped carbon semiconductor from rice husk char, Mater. Chem. Phys. 109 (2008) 169–173.
[49] S.K. Singh, B.C. Mohanty, S. Basu, Synthesis of SiC from rice husk in a plasma reactor, Bull. Mater. Sci. 25 (6) (2002) 561–563.
[50] B. Karmakar, P. Kundu, S. Jana, R.N. Dwiredi, Crystallization kinetics and mechanism of low expansion lithium-alumino-silicate glass ceramics by dilatometry, J. Am. Ceram. Soc. 85 (10) (2002) 2572–2574.
[51] M. Chatterjee, M.K. Naskar, Sol–gel synthesis of lithium aluminum silicate powders; the effect of silica sources, Ceram. Int. 32 (2006) 623–632.
[52] E. El-Fadaly, I.M. Bakr, M.R. Abo Breka, Recycling of ceramic industry wastes in floor tiles recipes, J. Am. Sci. 6 (10) (2010) 241–247.
[53] K.A. Matori, M.M. Haslinawati, Z.A. Wahab, H.A.A. Sidek, T.K. Ban, W.A.W.A.K. Ghani, Producing amorphous white silica from rice husk, J. Basic Appl. Sci. 1 (October (3)) (2009) 512–515.
[54] ASTM C114-00, Standard Test Methods for Chemical Analysis of Materials, ASTM International, 2009.
[55] S.M. Mirhadi, A. Forghani, F. Tavangarian, A modified method to synthesize single-phase forsterite nanoparticles at low temperature, Ceram. Int. 42 (2016) 7974–7979.
[56] C. Klein, C. Hurlbut Jr., Manual of Mineralogy, 20th ed., Wiley, 1985, pp. 373–375.
[57] M.T. Tsai, Hydrolysis and condensation of forsterite precursor alkoxides: modification of the molecular gel structure by acetic acid, J. Non-Cryst. Solids 298 (2002) 116–130.